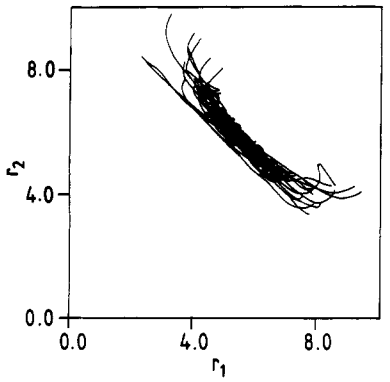

Figure 14. The center-of-cage to center-of-mass (coc–com) distance just before, during, and after cage-to-cage diffusion of methane near 300 K. The coc–com distance for the parent cage is r_1. Here, the parent cage is cage where the methane is residing before cage-to-cage diffusion. The coc–com distance for the daughter cage into which the molecule has migrated is given by r_2.

a neighboring cage. The coc–com distance between the methane and the daughter cage into which the molecule has migrated is r_2. Figure 14 shows a plot of r_1 against r_2 for several occurrences of the cage-to-cage migration. It is observed that r_1 and r_2 are always greater than or equal to 3.5 Å. Thus, the molecules always remain close to the inner surface of the parent cage as well as the daughter cage. The picture indicated by Figure 14 is that of a molecule skating on the surface of an α-cage. A detailed study of this has been recently carried out on xenon in faujasite.[37] It is clear that surface diffusion plays the dominant role in cage-to-cage migration of this molecule.

3.4. Conclusions. The calculated thermodynamic, equilibrium, and transport properties and frequency spectra are in good agreement with the experimentally available data. The guest preferentially occupies the region near the inner surface of the α-cage. This seems to be a general characteristic of adsorption in faujasites irrespective of the guest.[18] The positions of the bands in the power spectra obtained by Fourier transformation of the com velocity autocorrelation function show a shift toward higher frequency with (a) decrease in temperature and (b) increase in concentration. There are three bands at 36, 53, and 85 cm^{-1} for the power spectra for the com motion and two bands at 95 and 150 cm^{-1} for the power spectra for the rotational motion about the com at 50 K and $n = 6$ molecules/cage. At higher loadings there is an increase in the population near the cage center. At lower loadings, especially $n = 2$ molecules/cage, the methanes seem to occupy preferentially certain regions near the cage surface leading to a significant number of guests with $-22 < U_{gh} < -17$ kJ mol^{-1}, i.e. in the proximity of the adsorption site. As a consequence of this, the C–Na rdf shows well-defined structures in the rdfs at low loadings which disappear at higher loadings. Cage-to-cage migration takes place by a sort of skating type of motion with the guest always near the inner surface of the α-cage. After this manuscript was submitted we found that a detailed study relevant to the present study of model systems and methane and xenon in faujasite has been studied by the grand canonical Monte Carlo method.[38,39] A number of other related studies have also appeared in print recently.[40]

Acknowledgment. The research outlined herein was supported, in part, by the U.S. National Science Foundation and the donors of the Petroleum Research Fund, administered by the American Chemical Society. M.L.K. thanks the John Simon Guggenheim Memorial Foundation for the award of a Fellowship.

(37) Yashonath, S. *J. Phys. Chem.*, in press.

(38) Woods, G. B.; Rowlinson, J. S. *J. Chem. Soc., Faraday Trans. 2* **1989**, *85*, 765.
(39) Rowlinson, J. S.; Woods, G. B. *Physica A* **1990**, *164*, 117.
(40) Titiloye, J. O.; Parker, S. C.; Stone, F. S.; Catlow, C. R. A. *J. Phys. Chem.* **1991**, *95*, 4038.

Predicting Molecular Structures of Surface Metal Oxide Species on Oxide Supports under Ambient Conditions

Goutam Deo and Israel E. Wachs*

Zettlemoyer Center for Surface Studies, Department of Chemical Engineering, Lehigh University, Bethlehem, Pennsylvania 18015 (Received: August 20, 1990)

The molecular structures of the two-dimensional vanadium oxide overlayers on different oxide supports (MgO, Al_2O_3, ZrO_2, TiO_2, and SiO_2) were determined with Raman spectroscopy under ambient conditions. The surface vanadium oxide molecular structures were found to depend on the net pH at which the surface possesses zero surface charge (point of zero charge, pzc). The net surface pH at pzc is determined by the specific oxide support and the surface coverage of the acidic vanadium oxide overlayer. Under ambient conditions the surface of the oxide support is hydrated and the surface vanadium oxide overlayer is essentially in an aqueous medium. Hence, the structure of the vanadium oxide overlayer follows the vanadium(V) oxide aqueous chemistry as a function of net pH at pzc and vanadium oxide concentration. The influence of calcination temperature and preparation methods as well as the addition of acidic and basic promoters upon the surface vanadium oxide molecular structures can also be understood and predicted from this model. The net surface pH at pzc was also successfully used to predict the molecular structures of surface rhenium oxide species, surface chromium oxide species, surface molybdenum oxide species, and surface tungsten oxide species on various oxide supports under ambient conditions.

Introduction

Many recent studies have demonstrated that two-dimensional metal oxide overlayers are formed when one metal oxide component (i.e., Re_2O_7, CrO_3, MoO_3, WO_3, V_2O_5, etc.) is deposited on a second high-surface-area metal oxide substrate (i.e., Al_2O_3, TiO_2, SiO_2, etc.).[1-5] The molecular structures of these surface metal oxide species have been extensively investigated over the past decade because of their importance in numerous catalytic

(1) Haber, J. In *Surface Properties and Catalysis by Non-Metals*; Bonnelle, J. B., Delmon, B., Devoune, E., Eds.; Reidel: Dordrecht, The Netherlands, 1983; p 1.

0022-3654/91/2095-5889$02.50/0

TABLE I: Support Specifications

support	supplier	surf. area, m^2/g
MgO	Fluka	80
γ-Al_2O_3	Harshaw	180
ZrO_2	Degussa	39
TiO_2	Degussa	55
SiO_2	Cabot	300

applications.[6] The major structural information about these surface metal oxide species has been derived from Raman spectroscopy studies because of the molecular nature of this characterization method and its ability to discriminate between different molecular species that may simultaneously be present in the sample.[2-5] More recently, X-ray absorption techniques (EXAFS/XANES) and solid-state NMR studies have also been applied toward the determination of the molecular structure of these surface metal oxide species on oxide supports. The X-ray absorption studies focused on surface vanadium oxide,[7] surface molybdenum oxide,[8] surface tungsten oxide,[9] surface rhenium oxide,[10] surface chromium oxide,[11] and surface niobium oxide.[12] The solid-state NMR characterizations have been limited to surface vanadium oxide due to the very favorable magnetic properties of the vanadium-51 nucleus.[13-15] These molecular structural characterization studies have revealed that the nature of the surface metal oxide species is dependent on the specific oxide support, surface coverage, extent of surface hydration, presence of impurities, and calcination temperature. The origins of these structural changes, however, are not well understood.

In the present investigation, the influence of the specific oxide support material upon the molecular structures of surface vanadium oxide overlayers is examined with Raman spectroscopy under ambient conditions, where the surface metal oxide species are known to be hydrated by adsorbed moisture.[16] This study focuses on the molecular structures under ambient conditions because, with few exceptions, all the prior investigations were limited to ambient characterization studies. The oxide support materials chosen for this investigation are MgO, Al_2O_3, ZrO_2, TiO_2, and SiO_2 because of their widely varying surface properties.[17] A model is developed that allows for the prediction of the molecular structures of the surface vanadium oxide overlayers as well as other metal oxide species (rhenium oxide, tungsten oxide, molybdenum oxide, chromium oxide, etc.) on oxide supports under ambient conditions.

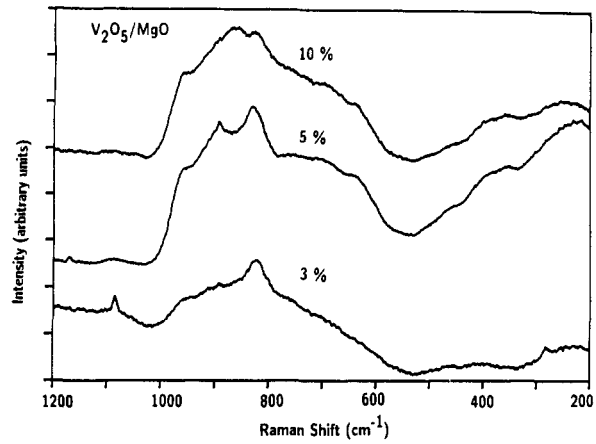

Figure 1. Raman spectra of V_2O_5/MgO as a function of V_2O_5 loading (surface coverage).

Experimental Section

The support materials used in this study are MgO, Al_2O_3, ZrO_2, TiO_2, and SiO_2. The MgO support was obtained as $Mg(OH)_2$ and was calcined at 700 °C for 2 h to convert the hydroxide to the oxide. The rest of the supports were calcined at 450/500 °C for 16 h before preparation of the samples. The supplier and surface area of the oxide supports after calcination are shown in Table I.

The vanadium oxide overlayers were prepared on the various oxide supports by the incipient wetness impregnation technique. Vanadium triisopropoxide oxide (Alfa, 95–98% purity) or vanadium triethoxide oxide was used as the vanadia precursor. The air- and moisture-sensitive nature of the alkoxide precursors required the preparation to be performed under a controlled environment. Solutions of the vanadium oxide precursors and methanol (Fisher, certified ACS, 99.9% pure) were made under flowing nitrogen and thoroughly mixed with the supports. The samples were dried overnight at room temperature and subsequently heated to 120 °C under a nitrogen atmosphere. The final calcination was performed in O_2 (Linde, 99.99% pure) at 450/500 °C. Details of the preparation of supported vanadium oxide overlayers have been described elsewhere.[18] All samples are reported as weight percent of V_2O_5 in the sample.

Laser Raman spectra were obtained with an Ar^+ laser (Spectra Physics, Model 2020-50). The incident laser line was tuned at 514.5 nm and delivered 1–100 mW of power measured at the sample. The scattered radiation from the sample was directed into an OMA III (Princeton Applied Research, Model 1463) optical multichannel analyzer with a photodiode array cooled thermoelectrically to −35 °C. All the Raman spectra were obtained under ambient conditions. Additional details about the laser Raman apparatus can be found elsewhere.[2]

Results

Oxide Supports and Vanadium Oxide Reference Compounds. The Raman active vibrations of most metal oxides lie in the 100–1200 cm^{-1} region. Consequently, it is necessary to know the

(2) Wachs, I. E.; Hardcastle, F. D.; Chan, S. S. *Spectroscopy (Eugene, Oreg.)* **1986**, *1*, 30.
(3) Dixit, L.; Gerrard, D. L.; Bowley, H. *Appl. Spectrosc. Rev.* **1986**, *22*, 189.
(4) Bartlett, J. R.; Cooney, R. P. In *Spectroscopy of Inorganic-based Materials*, Clark, R. J. H., Hester, R. E., Eds.; Wiley: New York, 1987; p 187.
(5) Hardcastle, F. D.; Wachs, I. E. *Proc.—Int. Congr. Catal., 9th* **1988**, *3*, 1449.
(6) Thomas, C. L. *Catalytic Processes and Proven Catalysts*; Academic Press: New York, 1970.
(7) (a) Kozlowski, R.; Pettifer, R. F.; Thomas, J. M. *J. Phys. Chem.* **1983**, *87*, 5176. (b) Haber, J.; Kozlowska, A.; Kozlowski, R. *J. Catal.* **1986**, *102*, 52. (c) Haber, J.; Kozlowska, A.; Kozlowski, R. *Proc.—Intern. Congr. Catal., 9th* **1988**, *4*, 1481. (d) Tanaka, T.; Yamashita, H.; Tsuchitani, R.; Funabiki, T.; Yoshida, S. *J. Chem. Soc., Faraday Trans. 1* **1988**, *84* (9), 2987. (e) Yoshida, S.; Tanaka, T.; Nishimura, Y.; Mizutani, H.; Funabiki, T. *Proc.—Int. Congr. Catal., 9th* **1988**, *3*, 1473.
(8) (a) Chieu, N.-S.; Bauer, S. H.; Johnson, M. F. L. *J. Catal.* **1984**, *89*, 226. (b) Chieu, N.-S.; Bauer, S. H.; Johnson, M. F. L. *J. Catal.* **1986**, *98*, 32.
(9) Horsley, J. A.; Wachs, I. E.; Brown, J. M.; Via, G. H.; Hardcastle, F. D. *J. Phys. Chem.* **1987**, *91*, 4014.
(10) Hardcastle, F. D.; Wachs, I. E.; Horsley, J.; Via, G. *J. Mol. Catal.* **1988**, *46*, 15.
(11) Kozlowski, R. *Bull. Pol. Acad. Sci., Chem.* **1986**, *35* (9), 365.
(12) (a) Kobayashi, H.; Yamaguchi, M.; Tanaka, T.; Nishimura, Y.; Kawakami, H.; Yoshida, S. *J. Phys. Chem.* **1988**, *92*, 2516. (b) Nishimura, M.; Asakura, K.; Iwasawa, Y. *J. Chem. Soc., Chem. Commun.* **1986**, 1660. (c) Nishimura, M.; Asakura, K.; Iwasawa, Y. *Proc.—Int. Congr. Catal.* **1988**, *4*, 1842.
(13) (a) Eckert, H.; Wachs, I. E. *Mater. Res. Soc. Symp. Proc.* **1988**, *111*, 459. (b) Eckert, H.; Wachs, I. E. *J. Phys. Chem.* **1989**, *93*, 6796. (c) Eckert, H.; Deo, G.; Wachs, I. E.; Hirt, A. M. *Colloids Surf.* **1990**, *45*, 347.
(14) (a) Costumer, L. R.; Taouk, B.; Le Meur, M.; Payen, E.; Guelton, M.; Grimblot, J. *J. Phys. Chem.* **1988**, *92*, 1230. (b) Taouk, B.; Guelton, M.; Grimblot, J.; Bonnelle, J. P. *J. Phys. Chem.* **1988**, *92*, 6700.
(15) (a) Mastikhin, V. M.; Lapina, O. B.; Krasilnikov, V. N.; Ivakin, A. A. *React. Kinet. Catal. Lett.* **1984**, *24*, 119. (b) Mastikhin, V. M.; Lapina, O. B.; Simonova, L. G. *React. Kinet. Catal. Lett.* **1984**, *24*, 119. (c) Lapina, O. B.; Simakov, A. V.; Mastkhin, V. M.; Veniaminov, S. A.; Shubin, A. A. *J. Mol. Catal.* **1989**, *50*, 55.
(16) Chan, S. S.; Wachs, I. E.; Murrell, L. L.; Wang, L.; Hall, W. K. *J. Phys. Chem.* **1984**, *88*, 5831.
(17) (a) Park, G. A. *Chem. Rev.* **1965**, *65*, 177. (b) Park, G. A. *Adv. Chem. Ser.* **1967**, *61*, 121.
(18) (a) Deo, G.; Hardcastle, F. D.; Richards, M.; Wachs, I. E. *Prepr.—Am. Chem. Soc., Div. Pet. Chem.* **1989**, *34* (3), 529. (b) Deo, G.; Hardcastle, F. D.; Richads, M.; Wachs, I. E.; Hirt, A. M. In *Novel Materials in Heterogeneous Catalysis*; Baker, R. T. K., Murrell, L. L., Eds.; ACS Symposium Series 437; American Chemical Society: Washington, DC, 1990; p 317.

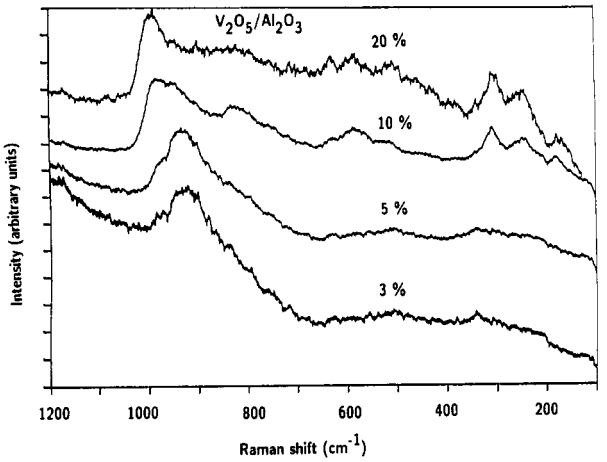

Figure 2. Raman spectra of V_2O_5/Al_2O_3 as a function of V_2O_5 loading (surface coverage).

Raman vibrations of the oxide support materials as well as those of vanadium oxide reference materials. The Raman spectra of the γ-Al_2O_3 support is featureless in the 100–1200-cm^{-1} region and does not interfere with the Raman vibrations of the supported metal oxide systems. The MgO support is essentially featureless except for a carbonate band at 1085 cm^{-1} that arises from some residual $MgCO_3$ present in the parent $Mg(OH)_2$. However, the TiO_2, ZrO_2, and SiO_2 supports are Raman active and possess Raman features in the 100–800-cm^{-1} region. The TiO_2 support has major Raman bands at 144, 199, 399, 448, 520, and 643 cm^{-1} and a weak band at 794 cm^{-1}. The ZrO_2 support has Raman features at 108, 182, 193, 224, 304, 331, 345, 378, 471, 497, 532, 554, 610, and 634 cm^{-1} and a weak band at 756 cm^{-1}. For SiO_2, broad Raman features are present at 432, 482, 608, 802, and 972 cm^{-1}. The Raman spectra of vanadium oxide reference materials have been described elsewhere, and the various coordinations and structures of vanadium oxide can be distinguished.[18] Solid-state ^{51}V NMR wide-line spectra of various vanadium oxide compounds have been shown to distinguish between the different coordinations of vanadium oxide[13a,b] and can be categorized into two different regions: octahedral species having chemical shifts −300 ppm and tetrahedral species having chemical shifts from −400 to −660 ppm.

V_2O_5/MgO. The Raman spectra of 3–10% V_2O_5/MgO are presented in Figure 1 and exhibit bands due to the vanadium oxygen stretch at ~820, 890, and 950 cm^{-1}, which are characteristic of orthovanadate (VO_4), pyrovanadate (V_2O_7), and metavanadate ($(VO_3)_n$), respectively.[18] Additional Raman bands due to the asymmetric and bending modes of the three species are present at ~760, ~640, ~340, and ~240 cm^{-1}. A chemical shift of −500 ppm is seen in the solid-state ^{51}V NMR wide-line spectra of these samples.[19] This confirms the presence of tetrahedrally coordinated vanadium oxide species and the complete absence of octahedrally coordinated vanadium oxide species on the MgO support. Thus, the supported vanadium oxide on MgO possesses surface orthovanadate, pyrovanadate, and to a lesser extent metavanadate species under ambient conditions, and their relative concentrations vary with surface coverage. The weak Raman band at 1085 cm^{-1} is due to the carbonate species on the MgO support.

V_2O_5/Al_2O_3. The Raman spectra of 3–20% V_2O_5/Al_2O_3 are presented in Figure 2 and possess major Raman bands in the 100–1000-cm^{-1} region. Above 20% V_2O_5/Al_2O_3, sharp Raman bands at 994, 700, 526, 481, 404, 305, 286, and 146 cm^{-1} are present which are indicative of microcrystalline V_2O_5 particles.[20] Consequently, a monolayer of the surface vanadium oxide species on this Al_2O_3 support (180 m^2/g) corresponds to ~20% V_2O_5. The weak and broad Raman bands in the 100–1000-cm^{-1} region are due to the surface vanadium oxide species on the alumina support. For 3 and 5% V_2O_5/Al_2O_3, a major Raman band is present at ~940 cm^{-1}, which is accompanied by weak bands at ~550, ~350, and ~220 cm^{-1}. These bands correspond to those found in polymeric tetrahedral vanadates and are due to surface metavanadate, $(VO_3)_n$, species.[18] This assignment is also in agreement with solid-state ^{51}V NMR studies that show the presence of tetrahedral vanadate species (chemical shift for solid-state ^{51}V NMR wide-line spectra of −550 ppm) possessing two bridging oxygens per vanadium atom.[13a,b] Above 5% V_2O_5/Al_2O_3, the major Raman band shifts to higher wavenumbers and a new strong and broad Raman band appears at 990–1000 cm^{-1}, as does a series of broad bands at 810–830, 550–580, ~500, 290–300, ~250, and ~180 cm^{-1}. Figure 3 presents the similarity between the Raman spectra of 10% V_2O_5/Al_2O_3 and the decavanadate ion in $Na_6V_{10}O_{28}\cdot 18H_2O$. Hence, the vanadium oxide species above 5% V_2O_5/Al_2O_3 is essentially the surface decavanadate, $V_{10}O_{28}^{6-}$, species.[18] Solid-state ^{51}V NMR studies support this conclusion since the NMR spectra are dominated by distorted, octahedrally coordinated vanadium oxide species (chemical shift for solid-state ^{51}V NMR wide-line spectra of −330 ppm) in this range.[13b] Thus, the two-dimensional vanadium oxide overlayer on the Al_2O_3 support under ambient conditions possesses surface metavanadate and decavanadate species and their relative concentrations vary with surface vanadium oxide coverage.

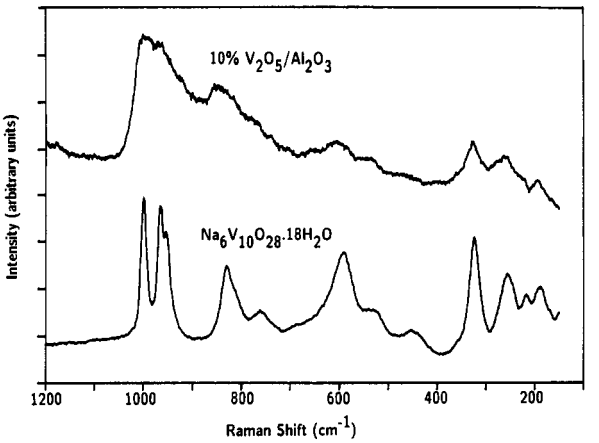

Figure 3. Raman spectra of 10%V_2O_5/Al_2O_3 and $Na_6V_{10}O_{28}\cdot 18H_2O$.

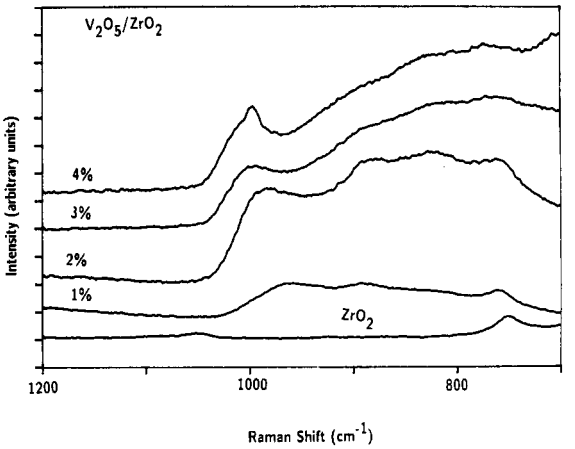

Figure 4. Raman spectra of V_2O_5/ZrO_2 as a function of V_2O_5 loading (surface coverage).

V_2O_5/ZrO_2. The Raman spectra of 1–4% V_2O_5/ZrO_2 are presented in Figure 4 and possess surface vanadium oxide bands in the 800–1000-cm^{-1} region. Strong Raman features due to the ZrO_2 phase limit the collection of data to above 700 cm^{-1}. The Raman spectrum above 700 cm^{-1} of the ZrO_2 support is included as a reference. A trace of crystalline V_2O_5 is present in the 4% V_2O_5/ZrO_2 sample, suggesting that this sample possesses slightly more than monolayer coverage. At low vanadium oxide coverage (1% V_2O_5/ZrO_2), Raman bands are observed at ~890 cm^{-1}, corresponding to pyrovanadate, and ~960 cm^{-1}, corresponding

(19) Eckert, H.; Deo, G.; Wachs, I. E. To be published.
(20) Wachs, I. E.; Hardcastle, F. D.; Chan, S. S. *Mater. Res. Soc. Symp. Proc.* **1988**, *111*, 353.

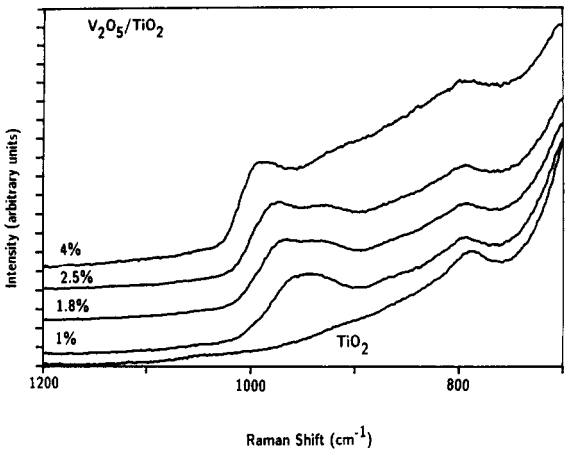

Figure 5. Raman spectra of V_2O_5/TiO_2 as a function of V_2O_5 loading (surface coverage).

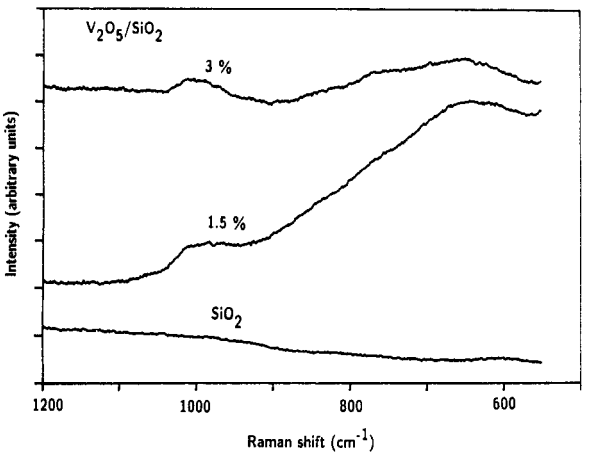

Figure 6. Raman spectra of V_2O_5/SiO_2 as a function of V_2O_5 loading (surface coverage).

to a mixture of metavanadate and decavanadate species. The Raman band at 756 cm^{-1}, present at low vanadium oxide loadings, is due to the ZrO_2 substrate and is masked at higher vanadium oxide coverage by the colored vanadium oxide overlayer. At low loadings (1% V_2O_5/ZrO_2) the solid-state ^{51}V NMR wide-line spectrum possesses a chemical shift at −510 ppm corresponding to tetrahedral vanadium oxide species.[19] At high vanadium oxide coverages (3% V_2O_5/ZrO_2), a broad Raman band is present at 990–1000 cm^{-1}, which is typical of the decavanadate, $V_{10}O_{28}^{6-}$, species. The V_2O_5/ZrO_2 Raman features are very similar to those found for the V_2O_5/Al_2O_3 system. Both systems show the presence of metavanadate and decavanadate species. An additional feature for the V_2O_5/ZrO_2 system is the presence of the pyrovanadate species at low loadings. At high loadings (3% V_2O_5/ZrO_2) the solid-state ^{51}V NMR wide-line spectra possess chemical shifts at −310 ppm (octahedral species) and −650 ppm (tetrahedral species) of which the octahedral species is the major component.[19] Thus, the two-dimensional vanadium oxide overlayer on the ZrO_2 support possesses surface metavanadate, surface pyrovanadate, and surface decavanadate species under ambient conditions, and their relative concentrations vary with surface vanadium oxide coverage.

V_2O_5/TiO_2. The Raman spectra of 1–4% V_2O_5/TiO_2 are presented in Figure 5 and possess bands in the 900–1000-cm^{-1} region. Raman spectra below 700 cm^{-1} are not collected because the very strong scattering from the TiO_2 support dominates this region. The Raman spectrum of the TiO_2 support above 700 cm^{-1} is included as a reference. The weak Raman feature at 794 cm^{-1} is also due to the TiO_2 substrate. Crystalline V_2O_5 Raman bands are present in the 7% V_2O_5/TiO_2 sample indicating that monolayer coverage of surface vanadium oxide has been exceeded.[20] At low vanadium oxide loadings two bands are observed at ~940 and 990–1000 cm^{-1}, and at high vanadium oxide loadings the band at 990–1000 cm^{-1} dominates. These Raman bands are the same as those observed for the V_2O_5/Al_2O_3 system, and this is confirmed by the solid-state ^{51}V NMR measurements, which also exhibit the characteristic features of surface metavanadate (chemical shift of −550 ppm) and surface decavanadate (chemical shift of −330 ppm) species.[13b] Unlike the V_2O_5/Al_2O_3 systems, the V_2O_5/TiO_2 system does not exclusively form the surface metavanadate species at low coverages. Comparison of the V_2O_5/Al_2O_3 and V_2O_5/TiO_2 spectra suggests that the surface decavanadate species is more dominant on the TiO_2 support than on the Al_2O_3 support. This is also observed in solid-state ^{51}V NMR.[13b] Thus, the two-dimensional vanadium oxide overlayer on the TiO_2 support possesses surface metavanadate and surface decavanadate species under ambient conditions and their relative concentrations vary with surface vanadium oxide coverage.

V_2O_5/SiO_2. The Raman spectra of 1.5 and 3.0% V_2O_5/SiO_2 are shown in Figure 6 along with the SiO_2 support. The spectra were collected at ~2 mW laser power. The hydrophobic nature of the silica support tends to dehydrate the surface vanadium oxide species on SiO_2 (laser-induced dehydration) at high laser powers.

TABLE II: Relative Amounts of Surface Vanadium Oxide Species on Different Oxide Supports under Ambient Conditions

support	VO_4	V_2O_7	$(VO_3)_n$	$V_{10}O_{28}$
MgO	high	high	low	none
γ-Al_2O_3	none	none	high	high
ZrO_2	none	low	high	high
TiO_2	none	none	low	high
SiO_2	none	none	none	high

No crystalline bands of V_2O_5 are detected at these vanadium oxide loadings. A broad Raman band is present at ~1000 cm^{-1} along with a band at ~650 cm^{-1}. A shoulder at ~750 cm^{-1} is also present for the 3% V_2O_5/SiO_2 sample, which may not be visible for the 1.5% V_2O_5/SiO_2 sample. No vibrations corresponding to SiO_2 were detected in the 550–1200-cm^{-1} region at this laser power. The Raman band at ~1000 cm^{-1} is typical of octahedrally coordinated vanadium oxide species in a decavanadate environment. The solid-state ^{51}V NMR wide-line spectrum of 1% V_2O_5/SiO_2 possesses a chemical shift of −300 ppm, which further confirms the presence of an octahedral species.[19] Conclusions from UV-vis[21] and EXAFS/XANES[7d] work on V_2O_5/SiO_2 samples also indicate the presence of VO_5 and octahedral surface vanadium oxide.

Discussion

Supported Vanadium Oxide Molecular Species. The Raman spectra reveal that the molecular structures of the surface vanadium oxide species under ambient conditions depend on the specific oxide support as well as the surface vanadium oxide coverage. Increasing the surface vanadium oxide coverage on a given oxide support always forms more polymerized and complex surface vanadium oxide species: orthovanadate (VO_4) → pyrovanadate (V_2O_7) → metavanadate $(VO_3)_n$ → decavanadate ($V_{10}O_{28}$). The oxide supports can be categorized into different groups based on the relative amounts of these species, as shown in Table II. Thus, MgO exhibits a preference for the formation of tetrahedrally coordinated surface vanadium oxide species (VO_4, V_2O_7), Al_2O_3 possesses a preference for the formation of surface vanadium oxide species tetrahedrally coordinated ($(VO_3)_n$) at low coverages and octahedrally coordinated ($V_{10}O_{28}$) at high coverages, and the remaining oxide supports have a high preference for the formation of octahedrally coordinated surface vanadium oxide species ($V_{10}O_{28}$).

The surface vanadium oxide species found on the various oxide supports under ambient conditions are also present in vanadium oxide aqueous solutions.[22] The common molecular vanadium oxide species in these two situations is not coincidental, since under

(21) Lishke, G.; Hanke, W.; Jerschkewitz, H.-G.; Ohlmann, H. *J. Catal.* **1985**, *91*, 54.
(22) Baes, C. F., Jr.; Mesmer, R. E. *The Hydrolysis of Cations*; Wiley: New York, 1970.

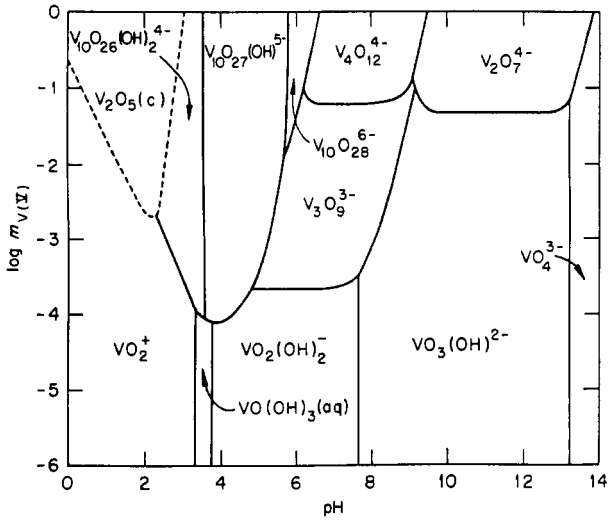

Figure 7. The different vanadium (V) oxide species present in aqueous solutions at 25 °C and I = 1 m. Reprinted with permission. (Baes, C. F., Jr.; Mesmer, R. E. *The Hydrolysis of Cations*; Wiley: New York, 1970.)

TABLE III: Predicted and Observed Vanadium Oxide Species on Different Oxide Supports. Low Vanadium Oxide Loadings

oxide support	pH	predicted low coverages	observed low coverages
MgO	11	$VO_3(OH)$	VO_4,[a] V_2O_7, $(VO_3)_n$
Al_2O_3	8.9	$VO_3(OH)$, $(VO_3)_n$	$(VO_3)_n$[a]
ZrO_2	5.9–6.1	$VO_2(OH)_2$, $(VO_3)_n$	V_2O_7, $(VO_3)_n$,[a] $V_{10}O_{28}$[a]
TiO_2	6.0–6.4	$VO_2(OH)_2$, $(VO_3)_n$	$(VO_3)_n$,[a] $V_{10}O_{28}$[a]
SiO_2	3.9	$V_{10}O_{26}(OH)_2$, $VO(OH)_3$	O_h[b]

[a] Major species. [b] Decavanadate-like environment, from solid-state ^{51}V NMR spectroscopy.[19]

ambient conditions the surfaces of the supported metal oxides are hydrated.[2,16] In aqueous solutions, the specific vanadium oxide species that can exist depend on the solution pH and vanadium oxide concentration.[22] The vanadium oxide aqueous phase diagram is shown in Figure 7. Decreasing the solution pH or increasing the vanadium oxide concentration results in formation of more polymerized and complex vanadium oxide species. Thus, it is not surprising that increasing the surface vanadium oxide coverage on a given oxide support, analogous to increasing the vanadium oxide concentration in solution, results in the formation of more polymerized and more complex surface vanadium oxide species.

The differences between the various oxide supports can be better understood by comparing the observed results for the hydrated surface vanadium oxide overlayers with changes in solution pH (see Figure 7). The surface vanadium oxide species observed on MgO are similar to those present in basic aqueous solutions (VO_4, V_2O_7, and the analogous hydroxylated species). The surface vanadium oxide species present on Al_2O_3 are similar to those found in slightly basic and slightly acidic aqueous solutions ($(VO_3)_n$, $V_{10}O_{28}$, and the analogous hydroxylated species). The surface vanadium oxide species present on TiO_2, ZrO_2, and SiO_2 are similar to those found in acidic aqueous solutions (primarily $V_{10}O_{28}$ and its hydroxylated analogues). Thus, the various oxide supports appear to be imposing different effective surface pH's on the hydrated surface vanadium oxide overlayer.

Aqueous solutions containing oxide materials gravitate toward the point of zero surface charge (pzc) of the oxide because oxide surfaces are positively charged at pH values below their pzc and negatively charged at pH values above their pzc.[23] Consequently, under ambient conditions the pH values of the hydrated oxide surfaces present on the oxide supports should be close to pzc of the specific oxide support. The pH values corresponding to pzc values for MgO, Al_2O_3, TiO_2, ZrO_2, and SiO_2 are listed in Table III. As can be seen from Table III, the pH values at pzc of the oxide supports range from ~3 to 11. On the basis of this scale, acidic oxides can be regarded as having pH < 7 at pzc and basic oxides as having pH > 7 at pzc, similar to acidic and basic solutions.

TABLE IV: Predicted and Observed Vanadium Oxide Species on Different Oxide Supports. High Vanadium Oxide Loadings

oxide support	pH	predicted high coverages	observed high coverages
MgO	11	$VO_3(OH)$, V_2O_7, $(VO_3)_n$	VO_4,[a] V_2O_7,[a] $(VO_3)_n$
Al_2O_3	8.9	V_2O_7, $(VO_3)_n$	$(VO_3)_n$, $V_{10}O_{28}$[a]
ZrO_2	5.9–6.1	$(VO_3)_n$, $V_{10}O_{27}(OH)$	$V_{10}O_{28}$[a]
TiO_2	6.0–6.4	$(VO_3)_n$, $V_{10}O_{28}$	$V_{10}O_{28}$[a]
SiO_2	3.9	$V_{10}O_{26}(OH)_2$, V_2O_5	V_2O_5

[a] major species.

An added factor contributing to the pH at pzc of the hydrated support oxide surfaces is the contribution of the vanadium oxide overlayer. The acidic characteristic of vanadium oxide (bulk V_2O_5 possesses a pzc at pH = 1.4[24]) in aqueous environments lowers the *net* surface pH at pzc. Gil-Llambias et al.[24] have shown that for the V_2O_5/TiO_2 and V_2O_5/Al_2O_3 systems, the pH at pzc of the samples decreases with increasing vanadium oxide loadings (surface vanadium oxide coverage). The effect of the surface vanadium oxide overlayer is especially pronounced at high vanadium oxide loadings. Hence, the pH at pzc of the supported vanadium oxide system is expected to be lower than the pH at pzc of the oxide support at high surface coverages and close to the oxide support at low surface coverages. The predicted surface vanadium oxide species based on the net pH at pzc of the surface and the known vanadium oxide aqueous phase diagram (Figure 7) are shown in Tables III and IV for low and high vanadium oxide loadings, respectively. At low surface vanadium oxide coverages the net pH at pzc should closely reflect the specific oxide support, and at high surface vanadium oxide coverages the net pH at pzc is significantly lowered due to the presence of the vanadium oxide overlayer. The qualitative agreement between the predicted surface vanadium oxide species and the observed surface vanadium oxide species on the different oxide supports, as seen in Tables III and IV, suggests that the net pH at pzc of each support is controlling the structure of these hydrated species.

Other Supported Metal Oxide Systems. The current finding that the surface vanadium oxide species present on hydrated oxide supports under ambient conditions can be correlated with the net pH at pzc of the oxide surface suggests that this approach should also hold for other surface metal oxide systems (Re_2O_7, CrO_3, MoO_3, and WO_3). Table V lists the observed surface metal oxide species found for rhenium oxide, chromium oxide, molybdenum oxide, and tungsten oxide on various oxide supports. Only monomeric ReO_4^- is present in aqueous solutions[22] and consequently, only ReO_4^- species would be expected on the hydrated oxide supports. Indeed, only monomeric ReO_4 is present, under ambient conditions, on all the oxide supports examined. Chromium oxide is present as CrO_4^{2-} in basic solutions and $Cr_2O_7^{2-}$ in acidic solutions.[22] Recently it was shown that at pH < 1 $Cr_3O_{10}^{2-}$ and $Cr_4O_{13}^{2-}$ also exist in aqueous solutions.[25] The observed surface chromium oxide species present on the hydrated oxide supports follow the trend predicted from the net pH at pzc correlation. Similarly, molybdenum oxide and tungsten oxide are present as MoO_4^{2-}/WO_4^{2-} in basic solutions and as polyoxoanions in acidic solutions ($Mo_7O_{24}^{6-}$ and $Mo_8O_{26}^{4-}/W_6O_{21}^{6-}$ and $W_{12}O_{39}^{6-}$).[22] Again, the observed surface molybdenum oxide and surface tungsten oxide species present on the hydrated oxide supports follow the trends predicted from the net pH at pzc. Thus, the net pH at pzc appears generally applicable for predicting the molecular structures of surface metal oxide species on hydrated oxide supports and can be applied to all hydrated supported metal oxide systems possessing two-dimensional metal oxide overlayers.

(23) Anderson, J. R. *Structure of Metallic Catalysts*; Academic Press: London, 1975.

(24) Gil-Llambias, F. J.; Escudey, A. M.; Fierro, J. L. G.; Agudo, A. L. *J. Catal.* **1985**, *95*, 520.

(25) Michel, G.; Chahay, R. *J. Raman Spectrosc.* **1986**, *17*, 4.

TABLE V: Observed Surface Metal Oxide Species on Different Oxide Supports[a]

oxide support	metal oxide			
	Re oxide	Cr oxide	Mo oxide	W oxide
MgO	ReO_4[b] (971)	CrO_4[b] (885)	MoO_4[b] (909)	WO_4[b] (935)
Al_2O_3	ReO_4[b] (981)	CrO_4,[b] Cr_2O_7 (896)	MoO_4, Mo_7O_{24}, Mo_8O_{26}[b] (958)	WO_4, $W_{12}O_{39}$[b] (960)
ZrO_2	ReO_4[b] (971)	CrO_4,[b] Cr_2O_7 (865)	Mo_7O_{24}, Mo_8O_{26}[b] (960)	WO_4, $W_{12}O_{39}$[b] (950)
TiO_2	ReO_4[b] (981)	CrO_4,[b] Cr_2O_7 (880)	MoO_4, Mo_7O_{24}, Mo_8O_{26}[b] (960)	WO_4, $W_{12}O_{39}$[b] (960)
SiO_2	ReO_4[b] (971)	Cr_2O_7, Cr_3O_{10},[b] Cr_4O_{13} (962)	Mo_7O_{24}[b] (944)	$W_{12}O_{39}$[b] (970)

[a] Raman band of major surface metal oxide species shown in parentheses. [b] Major species at monolayer coverage.

Effect of Surface Impurities/Promoters. Surface impurities/promoters should also influence the final surface vanadium oxide molecular structures since their presence should change the pH at pzc of the hydrated supported metal oxide. Basic impurities will increase the aqueous pH at pzc and acidic impurities will decrease the aqueous pH at pzc.[17,26] This effect has recently been observed for V_2O_5/TiO_2 and V_2O_5/Al_2O_3 catalysts contaminated with alkaline impurities (Na, K).[13c,18] The presence of surface sodium oxide and potassium oxide impurities were found to selectively favor the formation of surface orthovanadate species rather than surface metavanadate and decavanadate species. Upon adding acidic WO_3 and MoO_3 to V_2O_5/TiO_2 and V_2O_5/Al_2O_3, respectively, the preference for octahedral surface vanadium oxide species was observed at all vanadium oxide coverages.[19,27] This observation reveals the pronounced influence surface impurities/promoters have on the surface metal oxide structures of supported metal oxide catalysts under hydrated conditions.

Effect of Calcination Temperature. Calcination of the supported vanadium oxide samples at elevated temperatures usually reduces the surface area of the oxide support. The decrease in the surface area of the oxide support increases the surface vanadium oxide coverage and results in the reduction of the net pH at pzc of the hydrated oxide surface. Consequently, a mixture of metavanadate (~940 cm^{-1}) and decavanadate (990–1000 cm^{-1}) species on 1% V_2O_5/TiO_2 for samples calcined at 450 °C forms decavanadate (990–1000 cm^{-1}) species for the same sample calcined at 800 °C as the surface area reduces from 55 m^2/g to 11 m^2/g.[19]

Effect of Preparation. The above conclusion that the pH at pzc of an oxide support controls the molecular structures of hydrated surface metal oxide species under ambient conditions has very important implications for the preparation of such supported metal oxide catalytic materials. The current findings suggest that the same hydrated surface metal oxide species should form on an oxide support independent of the preparation method once the catalyst is exposed to ambient conditions. A series of MoO_3/TiO_2 and V_2O_5/TiO_2 catalysts were prepared by different methods. The different preparation methods and precursors used for making monolayer catalysts of V_2O_5/TiO_2 and MoO_3/TiO_2 were as follows: (1) aqueous impregnation for vanadium oxalate and molybdenum oxalate; (2) grafting for $VOCl_3$ and $MoCl_5$; (3) nonaqueous impregnation for vanadium alkoxide; (4) equilibrium adsorption for aqueous solutions of ammonium metavanadate and ammonium heptamolybdate; and (5) thermal spreading for physical mixtures of TiO_2 and V_2O_5 and of TiO_2 and MoO_3. All the preparation methods resulted in identical molecular species ($Mo_8O_{26}^{4-}$ and $V_{10}O_{28}^{6-}$) on the titania support according to Raman spectroscopy.[28] Similar observations were made for different preparations of MoO_3/SiO_2, MoO_3/Al_2O_3, and MoO_3/MgO catalysts.[29] The different preparation methods and precursors used were as follows: (1) aqueous methods (impregnation and equilibrium adsorption) for aqueous solutions of ammonium heptamolybdate and molybdenum oxalate; (2) nonaqueous methods (impregnation) for monomeric and dimeric allyls of molybdenum; (3) grafting for $MoCl_5$. Raman spectra of MoO_3/Al_2O_3 indicate the presence of MoO_4^{2-} (low loadings) and $Mo_7O_{24}^{6-}$ (high loadings). For MoO_3/SiO_2 and MoO_3/MgO samples, $Mo_7O_{24}^{6-}$ and MoO_4^{2-} species were observed, respectively. These studies confirm the above hypothesis that the preparation method will not affect the final molecular structures of the hydrated surface metal oxide species since the molecular structures are controlled by the pH at pzc. Only changes in the specific oxide support, calcination at elevated temperatures, and the presence of impurities/promoters can alter the surface metal oxide structures under ambient conditions.

Models of Hydrated Supported Metal Oxide Systems. Various models have been proposed to explain the properties of hydrated supported metal oxide systems. Roozeboom et al.[30] related the thermal stability of the surface vanadium oxide monolayer to the parameter Z/a. Z/a is the ratio of the carrier cation charge (Z) to the sum (a) of the ionic radii of the carrier cation and oxide anion (O^{2-}). No explanation, however, was given for the different molecular structures of surface vanadium oxide species. Leyrer et al.[31] proposed the isoelectric point of the support surface to be controlling the primary adsorption interactions for the surface molybdenum oxide species during equilibrium adsorption preparation. With respect to equilibrium adsorption preparation method, Wang and Hall[32] found that the anions present in solution are adsorbed on the surface of the metal oxide support and Meunier et al.[33] have shown that the adsorption of the metal oxide species from the aqueous solution takes place such that a parity of charge exists between the surface and the metal oxide ion. Mulcahy et al.[34] studied the adsorption of different metal oxide species from solution onto alumina and found different types of adsorption taking place. Spanos et al.[35] studied the adsorption behavior of molybdenum oxide onto alumina and found protonated surface hydroxyls to be responsible for adsorption. It is known, however, that the structure of the surface metal oxide changes upon heating to moderate calcination temperatures (450/500 °C), which are required to remove precursor/solvents. None of these studies have been able to provide a general explanation for the structure of the surface metal oxide species under hydrated conditions. The net surface pH at pzc model, on the other hand, satisfactorily explains the structure of the hydrated surface metal oxide species on metal oxide supports and provides a model for understanding the effects of impurities/promoters, calcination temperature, and preparation method.

Conclusions

The molecular structures of the two-dimensional vanadium oxide overlayers on different oxide supports (MgO, Al_2O_3, TiO_2, ZrO_2, and SiO_2) were determined under ambient conditions with Raman spectroscopy. The hydrated surface vanadium oxide molecular structures were found to depend on the net pH at pzc

(26) Vordonis, L.; Koustsoukos, P. G.; Lycourghiotis, A. *J. Chem. Soc., Chem. Commun.* **1984**, 1309.
(27) Vuurman, M. A.; Wachs, I. E.; Hirt, A. M. *J. Phys. Chem.*, submitted for publication.
(28) Machej, T.; Turek, A. M.; Haber, J.; Wachs, I. E. *Appl. Catal.*, in press.
(29) Williams, C.; Ekerdt, J.; Jehng, J. M.; Hardcastle, F. D.; Wachs, I. E. *J. Phys. Chem.*, submitted for publication.
(30) Roozeboom, F.; Fransen, T.; Mars, P.; Gellings, P. J. *Z. Anorg. Allg. Chem.* **1979**, *449*, 25.
(31) Leyrer, J.; Vielhaber, B.; Zaki, M. I.; Shuxin Zhuang; Weitkamp, J.; Knözinger, H. *Mater. Chem. Phys.* **1985**, *13*, 301.
(32) (a) Wang, L.; Hall, W. K. *J. Catal.* **1982**, *77*, 232. (b) Wang, L.; Hall, W. K. *J. Catal.* **1980**, *66*, 251.
(33) Meunier, G.; Mocaer, B.; Kasztelan, S.; Le Coustumer, L. R.; Grimblot, J. P. *Appl. Catal.* **1986**, *21*, 329.
(34) Mulcahy, F. M.; Fay, M. J.; Proctor, A.; Houlla, M.; Hercules, D. M. *J. Catal.* **1990**, *124*, 231.
(35) Spanos, N.; Vordonis, L.; Kordulis, Ch.; Lycourghiotis, A. *J. Catal.* **1990**, *124*, 301.

of the oxide surface. The net pH at pzc of the oxide surface depends on the specific oxide support and the vanadium oxide surface coverage. Oxide supports possessing a basic aqueous pH at pzc were found to predominantly form tetrahedral surface vanadium oxide species (orthovanadate, pyrovanadate, and metavanadate), and oxide supports possessing an acidic aqueous pH at pzc were found to predominantly form octahedral surface vanadium oxide species (decavanadate). Thus, MgO (pH at pzc = 12) has a high preference for the formation of tetrahedrally coordinated surface vanadium oxide species (VO_4, V_2O_7), Al_2O_3 (pH at pzc = 9) has a preference for the formation of tetrahedrally coordinated surface vanadium oxide species ($(VO_3)_n$) at low surface coverages and octahedrally coordinated surface vanadium oxide species ($V_{10}O_{28}$) at high surface coverages, and the remaining oxide supports (TiO_2, ZrO_2, and SiO_2), possessing pH's at pzc of 6.0-2.0 exhibit a high preference for the formation of octahedrally coordinated surface vanadium oxide species ($V_{10}O_{28}$).

The presence of surface impurities/promoters and calcination temperature can also influence the surface pH at pzc of the hydrated oxide support. Acidic impurities decrease the aqueous pH at pzc and basic impurities increase the aqueous pH at pzc of the surface. High calcination temperatures, when accompanied by a reduction in surface area, result in a higher surface vanadium oxide coverage and a reduction of the net pH at pzc of the hydrated surface. The current studies also suggest that the preparation method will not affect the final molecular structures of the surface metal oxide species because it cannot influence the final pH at pzc of the hydrated oxide surface. The pH at which the oxide support possesses net zero surface charge was also successfully used to predict the molecular structures of surface rhenium oxide species, surface chromium oxide species, surface molybdenum oxide species, and surface tungsten oxide species on various oxide supports under ambient conditions.

Acknowledgment. The stimulating discussions with K. Segawa, NMR results of H. Eckert, preparation of V_2O_5/MgO catalysts by C. K. Chen, Raman spectra of V_2O_5/Al_2O_3 from F. D. Hardcastle, pH at pzc measurements of the supports by J. Ekerdt, and the financial support by NSF CBT No. 8810714 are gratefully acknowledged.

Surface Diffusion at the Liquid-Solid Interface: Quenching of Fluorescence from Pyrene Covalently Bound to Methylated Silica

A. L. Wong and J. M. Harris*

Department of Chemistry, University of Utah, Salt Lake City, Utah 84112 *(Received: October 22, 1990; In Final Form: February 8, 1991)*

The rates of iodine quenching of fluorescence from immobilized pyrene on methylated and bare porous silica gels suspended in methanol and aqueous methanol solvents are measured and compared. The interfacial quenching rate of (3-(1-pyrenyl)propyl)dimethylmonochlorosilane (3PPS) on C1-modified silica in methanol is significantly larger than the rate observed on bare silica. The enhanced rate on C1 silica is attributed to surface transport whereby iodine quencher molecules adsorb onto the hydrophobic surface and diffuse laterally to collide with the excited pyrene probe. This mechanism is supported by chromatographic data indicating that adsorbed iodine on the C1 silica is 100 times higher in concentration than on bare silica. From the surface concentrations of iodine determined chromatographically, rate constants for surface diffusion quenching and surface diffusion coefficients are estimated. Surface diffusion coefficients of iodine at a liquid/solid interface are found to be 2-3 orders of magnitude smaller than for diffusion in bulk solution, the differences of which depend on the composition of the overlying solvent.

Introduction

Studies of reaction kinetics of molecules adsorbed from solution to solid surfaces have received the attention of many researchers in the past two decades. The interest in chemical reactions on surfaces arises from a desire to immobilize catalytic reaction centers, to modify selected reaction pathways at a surface, and to enhance the rates of molecular transport in lower dimensional environments. In order to increase surface activity relative to bulk chemistry, high surface area porous solids are often chosen as substrates for these applications. For example, the high surface area, stability, and diverse surface-derivatization chemistry of porous silica[1] makes it an ideal host for studying chemistry at surfaces. Researchers have also utilized silica as a model substrate to investigate reaction rates in porous solids.[2]

Luminescence spectroscopy is a powerful technique to study structure and transport of molecules in porous solids.[3,4] Length scales for molecular transport on the microsecond time scale of excited triplet state decay can be as large as 5000 Å for gas-phase diffusion. Diffusion of oxygen within porous silica has been probed by quenching of excited triplet states[5] monitored by time-resolved, diffuse-reflectance methods. Decay rates of triplet states of benzophenone adsorbed on the pore surface were related to diffusion rates of oxygen molecules, measured over distances as large as 50 times the average pore diameter. Comparing the measured quenching rate and the adsorption isotherm for oxygen indicated that quenching was entirely from the gas phase with no surface diffusion indicated. Triplet-triplet annihilation of naphthalene in porous silica has been studied by Kopelman and co-workers;[6] the results indicated a nonfractal surface topology. Energy transfer between triplet benzophenone and naphthalene adsorbed to silica shortens the triplet lifetime of the excited donor;[7] these results provided evidence of surface diffusion at the gas-solid interface

(1) Iler, R. K. *The Chemistry of Silica, Solubility, Polymerization, Colloid and Surface Properties, and Biochemistry*; John Wiley & Sons: New York, 1979.
(2) Thomas, J. K. *J. Phys. Chem.* **1987**, *91*, 267.
(3) Lakowicz, J. R. *Principles of Fluorescence Spectroscopy*; Plenum Press: New York, 1983.
(4) Drake, J. M.; Klafter, J. *Phys. Today* **1990**, (6), 46.
(5) Drake, J. M.; Levitz, P.; Turro, N. J.; Nitsche, K. S.; Cassidy, K. F. *J. Phys. Chem.* **1988**, *92*, 4680.
(6) Kopelman, R.; Parus, S.; Prasad, J. *Phys. Rev. Lett.* **1986**, *56*, 1742.
(7) Turro, N. J.; Zimmt, M. B.; Gould, I. R. *J. Am. Chem. Soc.* **1985**, *107*, 5826.

0022-3654/91/2095-5895$02.50/0